Catalysis Science & Technology

Accepted Manuscript

ROYAL SOCIETY OF CHEMISTRY

www.rsc.org/catalysis

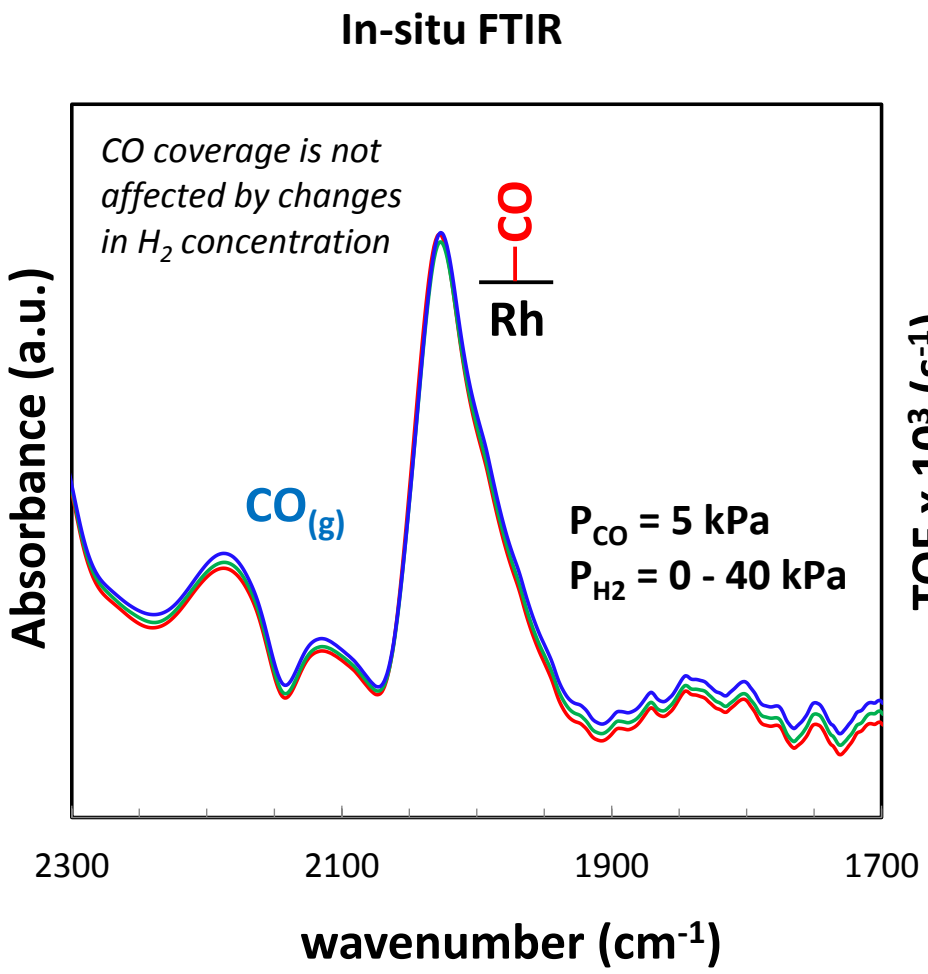

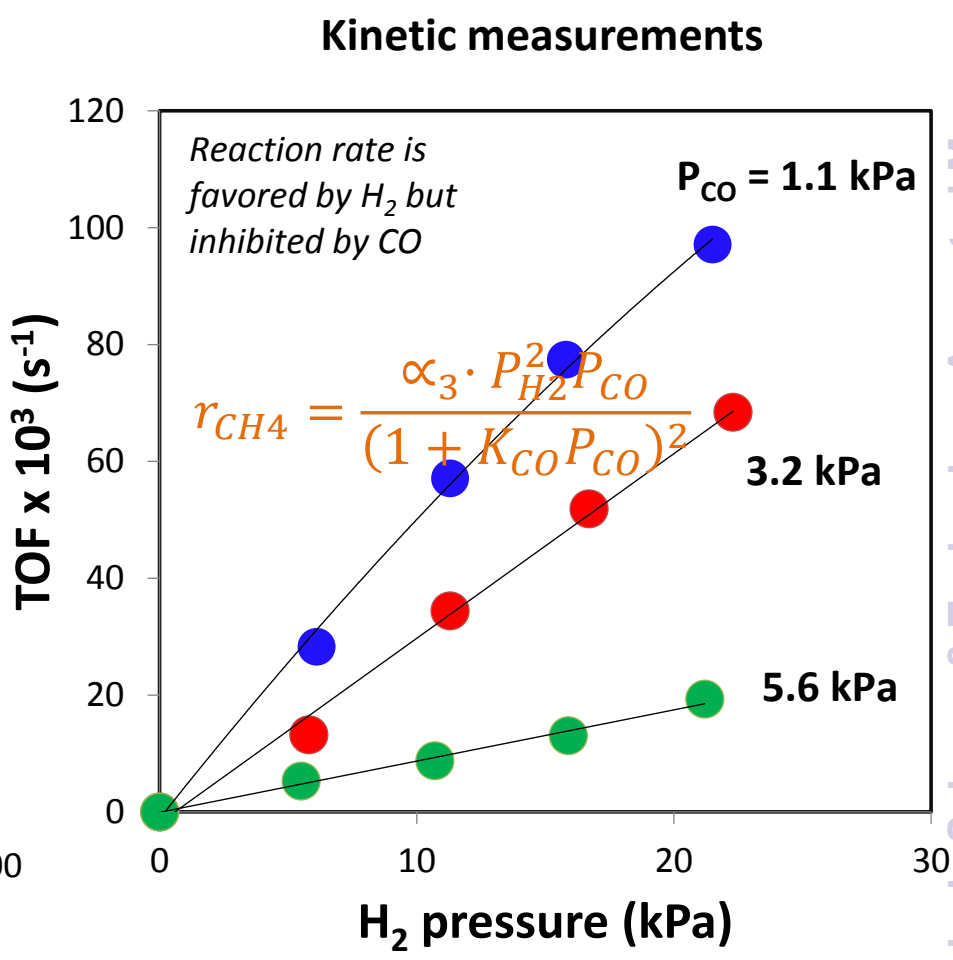

Kinetic and *in-situ* FTIR study of CO methanation on a Rh/Al_2O_3 catalyst.

Mauricio Escobar[a,c], *Francisco Gracia*[b], *Alejandro Karelovic*[a], *Romel Jiménez*[a*]

[a] Department of Chemical Engineering, Universidad de Concepción, Chile

[b] Department of Chemical Engineering and Biotechnology, Universidad de Chile, Chile

[c] Current address: Technological Development Unit (UDT) of the Universidad de Concepcion, Parque Industrial Coronel, Coronel, Chile

* Corresponding author: romeljimenez@udec.cl

ABSTRACT

Carbon monoxide hydrogenation was studied over a γ-alumina-supported 1 wt.% Rh catalyst by means of kinetic and in situ-Infrared measurements. The study was carried out at 200-300ºC, 0 – 22.5 kPa H_2 and 1 – 7.5 kPa CO. The *in-situ* FTIR scrutiny of catalyst surface shows that adsorbed CO* species and vacancies dominate the Rh surface, while no effect of H_2 and H_2O pressures on surface coverage was observed at the conditions studied. Kinetic data are consistent with a mechanism in which the C-O bond dissociation is assisted by a double H-addition while H_2 dissociative adsorption, CO molecular adsorption and the HCO* formation are quasi-equilibrated steps. A two-parameter Langmuir-Hinshelwood rate expression is deduced for CH_4 formation, in agreement with the proposed sequence of elementary steps and kinetic data. The effect of temperature on parameters α and K_{CO} leads to an apparent activation energy of 82.3 $kJ \cdot mol^{-1}$, an average CO adsorption enthalpy of -14.1 $kJ \cdot mol^{-1}$ and an entropy change of -17.9 $J \cdot mol^{-1} \cdot K^{-1}$. I*n-situ* FTIR experiments show a full coverage of Rh surface with adsorbed CO below 200ºC and this CO* coverage decreases as temperature increases in the range 200-300ºC; it is also observed that the heat of CO adsorption on Rh surface decreases with CO* coverage.

KEYWORDS: Carbon monoxide methanation, heat of CO adsorption, H*-assisted CO dissociation, in-situ FTIR, $Rh/\gamma\text{-}Al_2O_3$.

1. INTRODUCTION

The CO hydrogenation reaction to form methane (Eq.1) has been extensively studied over a wide variety of catalysts; the Group VIII metals have shown the highest activity for this reaction. The

activity has been related to both, the adsorption enthalpy of carbon monoxide, and the dissociation energy of the C-O bond of the adsorbed carbon monoxide molecule on the catalytic surface [1-5]. It is generally agreed that the dissociation of the C-O bond is the rate-limiting step for CO hydrogenation on Rh-based catalysts [6-9], and that the mechanism for CO hydrogenation is similar to that for CO_2 hydrogenation [6,10,11]. Less generally agreed upon is whether C-O bond cleavage occurs via the direct dissociation of adsorbed CO or via a hydrogen-assisted process.

$$CO + 3H_2 \rightarrow CH_4 + H_2O \qquad \Delta H^o_{rx} = -210\ kJ/mol \qquad (1)$$

Several authors have provided evidences supporting hydrogen assisted C-O bond dissociation. Fisher and Bell studied the CO and CO_2 hydrogenation over Rh/SiO_2 catalyst [6]. They proposed that the rate determining step (RDS) in the formation of methane is the H_2CO^* dissociation, produced by the stepwise hydrogenation of adsorbed CO. This mechanism is consistent with that proposed by Van Herwijnen et al. [7] and Vannice for CO hydrogenation on various Group VIII metals [12]. Karelovic and Ruiz studied the CO_2 methanation over Rh/Al_2O_3 catalysts [13]; they concluded that C-O bond dissociation of CO_{ads}, which is formed from CO_2 dissociative adsorption, is the rate-determining step, and suggest that H-aided C-O bond breaking is a key step in CO_2 methanation on these catalysts [13]. The existence of a strong H-D kinetic isotopic effect in CO methanation was attributed to the participation of H atoms in the rate determining step, in which a partially hydrogenated CO species is dissociated [8], which agrees with the H-assisted dissociation process proposed in other works [14,15].

On the other hand, Shetty and van Santen have presented theoretical calculations showing that direct CO dissociation has a lower activation barrier compared to H-assisted pathway over a Ru (1121) surface. The authors propose that the carbide mechanism would be thus preferred over Ru catalysts [16]. The unassisted CO dissociation has also been postulated in the case of CO methanation over Ni [9]. For Rh catalysts, it has also been proposed that CO is dissociated directly without assistance by hydrogen [17,18]. In fact, Iizuka et al. [18] proposed that the rate-determining step in the reaction of $CO+H_2$ involves the hydrogenation of partially hydrogenated CH_x and observed an inverse H/D kinetic isotope effect for $CO+H_2(D_2)$ reaction on ZrO_2- and Al_2O_3-supported Rh catalysts, which is attributed to the higher stability, and consequently concentration, of CD_x species as compared with CH_x after direct CO dissociation, leading to a higher rate-determining hydrogenation rate of deuterated species. In the same line, Orita et al. [32]

have reported that the first hydrogenation of carbon deposit is the rate determining step of CO methanation over Rh catalysts.

At CO methanation conditions, it is generally agreed that adsorbed CO is the most abundant intermediate. IR experiments have been used to show that CO is adsorbed on the metal surface with a significant coverage [6,7,21]. Some authors propose that vacant sites as well as adsorbed CO species are the dominant sites [7], whereas others take into account a significant coverage of adsorbed atomic hydrogen besides CO [6].

This work addresses the mechanism and kinetics of CO hydrogenation to produce CH_4 on a Rh(1 wt.%)/γ-Al_2O_3 catalyst. The issue whether CO is directly dissociated or assisted by H atoms is discussed on the basis of kinetic modelling. This work seeks to discriminate whether the CO dissociation follows the first or second H addition. Kinetic experiments and *in-situ* FTIR measurements permitted to assess the surface coverage of different intermediates and propose that vacancies and linearly adsorbed CO represent the most abundant reaction intermediates at the reaction conditions. The values for the equilibrium constant of CO adsorption and the corresponding CO adsorption enthalpies were calculated from *in-situ* FTIR measurements and from kinetic data at similar temperature and pressure conditions; thus, these parameters obtained from two independent measurements on the same catalysts at similar reaction conditions were compared in order to assess their physicochemical meaning and to validate the mechanism and kinetic model proposed for the CO hydrogenation reaction on supported Rh catalyst.

2. EXPERIMENTAL METHODS

2.1. Catalyst synthesis and characterization

The Rh catalysts were prepared by wet impregnation of pure γ-Al_2O_3 (Alfa Aesar, S_{BET} = 72 m^2/g). 5 g of the powdered support were immersed into deionized water and 180 mg of ammonium hexachlororhodate (Alfa Aesar, 28 wt.% of Rh) were added to the solution to obtain 1 wt.% Rh catalyst. After stirring for two hours at room temperature, the solvent was evaporated in a rotary evaporator at 35°C under reduced pressure. The resulting solid was dried at 110°C overnight and later calcined in air at 700°C for 4h. Atomic Absorption Spectroscopy confirmed the 1 wt.% Rh loading by using a Hitachi Z-8100 spectrometer with Zeeman polarization.

The amount of exposed Rh atoms was measured by irreversible hydrogen chemisorption in a homemade volumetric adsorption instrument equipped with a Dual-Gauge controller (TPG 262)

and a sensor APR 260 (0.1–1100 mbar, Pfeiffer Vacuum). Prior to H_2 adsorption, 800 mg of catalyst were in-situ reduced in pure H_2 at 700ºC for 2 h, flushed in He for 30 minutes and then cooled down to 30ºC. A first H_2 adsorption isotherm was measured at 30ºC, then the sample was isothermally evacuated for 2 h and a second isotherm was measured to quantify the reversibly adsorbed H_2. The irreversible hydrogen uptake was determined from the difference between the two isotherms. H/Rh = 1 stoichiometry was assumed to calculate the amount of exposed Rh atoms in the sample [14]. The average Rh cluster size was also determined from TEM, which confirmed the Rh particle size and dispersion estimated from H_2 chemisorption (TEM micrographs are not shown).

Transmission infrared spectra of self-supported Rh/Al_2O_3 wafers (~20 mg) were collected *in-situ* in a reactor cell placed in a FTIR spectrometer (Nicolet 6700, Thermo Scientific) at a resolution of 4 cm^{-1} and 50 scans/spectrum within the 3500 – 1500 cm^{-1} range. The IR cell is equipped with KBr windows, has connections for inlet and outlet flows, and thermocouples connected to a temperature controller to monitor and control its temperature. The spectra were obtained in absorbance mode after subtraction of the background spectrum of the catalyst disk under He atmosphere at the corresponding temperature. The samples (previously reduced at 700°C during 4h) were in situ pretreated in pure H_2 at 280ºC. After pretreatment, the catalyst surface was flushed with 100 ml/min of pure He, and the temperature was set to the study conditions. For adsorption/desorption experiments, 1.5 vol.% to 5 vol.% CO was added to the feed of pure He. For reaction conditions a mixture of CO and H_2 in He was used. In both types of experiments the total flow was set to 100 ml/min. The space velocity used for in-situ FTIR experiments was ~ 8 times larger than the higher space velocity used for kinetic measurements in order to guarantee differential conditions and avoid concentration gradients across the catalyst wafer during IR experiments. The outlet stream from IR cell is coupled to the Mass Spectrometer (OmniStar, Pfeiffer Vacuum) in order to quantify the CO conversion and CH_4 formation during in-situ FTIR measurements. Thus, the low CO conversion (X<10%) was used to confirm the differential reactor behavior. In the case of experiments with water addition, a bubbling saturator working at 3 different temperatures was used. The desired water concentration was achieved by diluting the water-saturated stream with pure He flow.

2.2. Kinetic measurements

The catalyst was sieved and selected in the 53 - 106 μm fraction, and diluted with Al_2O_3 pellets with size between 140-250 μm (catalyst mass/total mass = 1:3), to reduce radial and axial temperature gradients in the bed. Catalytic tests were carried out using a quartz reactor (U-shaped) with 0.4 cm internal diameter. A section in the center of the tube is expanded with a diameter of 1 cm, in which the catalyst was placed and supported by a quartz frit. A thermocouple was in contact with the central part of the catalyst bed and was used to measure and control the temperature. The Madon-Boudart criterion [22] was used to rule out heat and mass transfer limitations in the catalytic bed; thus, it is assumed that the reaction took place in fully kinetic regime.

The catalyst was reduced by increasing the temperature (10°C/min) from room temperature to 700°C in pure H_2 (Indura S.A., >99.99%) flow (30 ml/min), kept at 700°C for 2h and cooled down to the reaction temperature. The reaction was carried out between 200-300°C in the flow reactor at atmospheric pressure. Reactant gases were obtained from Indura S.A. (10.7% CO/He, H_2, He, Ar, 99,99% purity). Before reaction, the catalyst surface was cleaned by increasing the temperature (10°C/min) from room temperature to 500°C in pure He (Indura S.A., >99.99%) flow (30 ml/min), and holding the sample at 500°C for 1.5 h. Reaction rates were determined for CO conversion lower than 10% to ensure differential reactor conditions.

The concentrations of CO in the inlet and CO, CO_2 and CH_4 in outlet streams were measured using a Mass Spectrometer (QMS 403C Aëolos, Netzsch). Signals at 28, 44 and 15 amu were used to quantify the CO, CO_2 and CH_4 concentration, respectively, from previously calibrated curves using the Argon signal (Indura S.A., 99.999% purity) as reference gas. A concentration of 15% Ar in the reactant mixture was fed for each kinetic experiment. H_2O concentration was determined from oxygen balances.

Reaction rates are reported as turnover rate (TOF), i.e., moles of CH_4 produced per mole of exposed Rh on the surface per second. The moles of Rh on the surface were obtained from H_2 chemisorption at 30ºC. Equation 2 is used to estimate the forward reaction rate (r_{fi}) from the measured net CH_4 formation rate (r_{ni}) and the approach to equilibrium parameter (η_i) is calculated from Eq.3.

$$r_{ni} = r_{fi}(1 - \eta_i) \quad (2)$$

$$\eta_{met} = \frac{[P_{CH4}][P_{H2O}]}{[P_{H2}]^3[P_{CO}]}\frac{1}{K_{met}} \quad (3)$$

$$\Delta G_r^\circ = -RT \cdot ln(K_{met}) \quad (4)$$

$[P_i]$ is the steady state pressure of each component in atm.

K_{met} is the equilibrium constant for CO hydrogenation reaction (Eq.1)

The values for K_{met} were calculated from the Gibbs free energy change for reaction (Eq.4), resulting $2.248 \cdot 10^{11}$, $1.182 \cdot 10^{9}$ and $1.553 \cdot 10^{7}$, at 200, 250 and 300ºC, respectively. The decrease of K_{met} with temperature is consistent with the exothermic nature of CO hydrogenation reaction. Thus, the approach to equilibrium parameter at 200, 250 and 300ºC results $1.967 \cdot 10^{-16}$, $2.727 \cdot 10^{-11}$ and $1.765 \cdot 10^{-7}$, respectively; consequently, the forward reaction rates (r_{fi}) were assumed to be equal to the measured net CH_4 formation rates (r_{ni}) at all conditions used in this kinetic study.

3. RESULTS AND DISCUSSION

3.1. Turnover rate measurements.

The kinetic measurements were performed at 200-300ºC on 1%Rh/Al_2O_3 catalyst with BET surface area of 59 m^2/g and Rh dispersion of 35%, which represents a mean Rh particle size of 3 nm. During the kinetic experiments, the initial reaction condition was tested again after several measurements of reaction rate at different steady state conditions and no deactivation was observed.

Figure 1 shows the turnover frequency (TOF) of methane formation as a function of CO and H_2 partial pressures, at 250°C (a) and 300°C (b). The rate of methane formation increases as the H_2 pressure is increased. Conversely, an increase in CO partial pressure leads to lower CH_4 formation rates (The turnover formation rate of CH_4 as a function of CO pressure is shown in section S1 of the Supporting Information associated to this manuscript). The rates shown in Figure 1 can be compared with data presented previously over Rh/Al_2O_3 catalysts. Typical values range from 4.1×10^{-3} s^{-1} to 4.7×10^{-3} s^{-1} at 250°C and from 30×10^{-3} s^{-1} to 35×10^{-3} s^{-1} at 300°C [12,14,17]. Those values were obtained at stoichiometric or near-stoichiometric H_2/CO ratios, and can be compared with the lower rates presented in Figure 1 (2.74×10^{-3} s^{-1} at 1.1 kPa H_2 and 4.9 kPa CO at 250°C; 28.3×10^{-3} s^{-1} at 1.1 kPa H_2 and 6.1 kPa CO at 300°C). The data thus agree qualitatively well. When high H_2/CO ratios are used, as in the selective CO methanation [19], CH_4 formation rates can be significantly higher. Reaction rates of 13×10^{-3} s^{-1} at 250°C and 112×10^{-3} s^{-1} at 300°C have

been reported for Rh/Al_2O_3 at a molar ratio $H_2/CO = 50$. It can be observed that these values agree well with the rates presented in Figure 1 at low CO pressures and high H_2 pressures.

Scheme 1 illustrates a methane formation mechanism through direct dissociation of adsorbed carbon monoxide with a Rh vacancy. The symbols ⇌, → and ⇔ represent the quasi-equilibrated, irreversible and reversible steps, respectively. From the results shown in Fig. 1, which demonstrate the positive effect of P_{H2} and the negative effect of P_{CO} on the CH_4 formation rate at the reaction conditions evaluated, the direct CO dissociation mechanism (Scheme 1) can be ruled out regardless the identity of most abundant surface intermediates (MASI) that could be considered in the site balance.

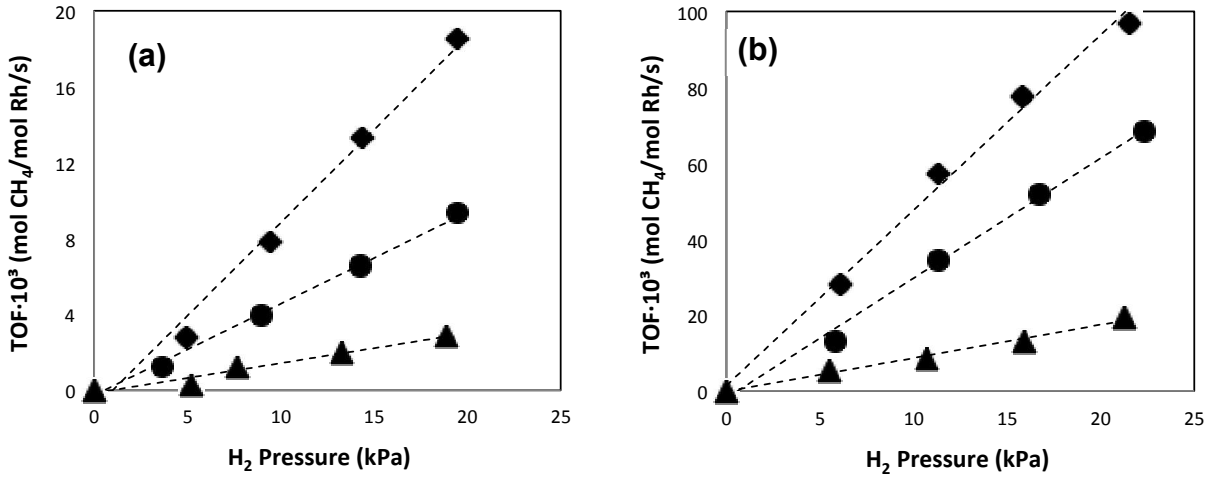

Figure 1. Forward turnover formation rate of CH_4 on Rh/Al_2O_3 as a function of H_2 and CO pressures at (a) 250ºC and (b) 300ºC. P_{H2} (0 – 22.5 kPa), Pco: (♦) 1.0 kPa, (●) 3.3 kPa, (▲) 5.5 kPa. Space velocity: 4 – 10 $cm^3 \cdot s^{-1} \cdot g_{cat}^{-1}$.

Reaction Scheme 1.

1.1) $CO + * \rightleftharpoons CO*$

1.2) $H_2 + 2* \rightleftharpoons 2H*$

1.3) $CO* + * \rightarrow C* + O*$

1.4) $C* + H* \rightarrow CH* + *$

1.5) $CH* + H* \rightarrow CH_2* + *$

1.6) $CH_2* + H* \rightarrow CH_3* + *$

1.7) $CH_3* + H* \rightarrow CH_4* + *$

1.8) $CH_4* \rightarrow CH_4 + *$

1.9) $O* + 2H* \rightarrow H_2O + 3*$

1.10) $O* + CO* \rightarrow CO_2 + 2*$

Scheme 1. Direct C-O bond dissociation mechanism. CO* specie reacts with an Rh vacancy.

In fact, this unassisted C-O bond dissociation mechanism would be consistent with a CH_4 formation kinetics of either negative order on P_{H2} if H* is a MASI (Eq.5) or independent of P_{H2} if adsorbed hydrogen is out of the site balance (Eq.6). Similar rate equations would be obtained for the CO disproportionation mechanism. A detailed derivation of these rate equations is provided in the section S2 of the Supporting Information associated to this manuscript.

$$r_{CH4} = \frac{kP_{CO}}{\left(1+K_{H2}^{0.5}P_{H2}^{0.5}+K_{CO}P_{CO}\right)^2} \quad (5)$$

$$r_{CH4} = \frac{kP_{CO}}{(1+K_{CO}P_{CO})^2} \quad (6)$$

Consequently, the direct (unassisted) C-O dissociation mechanism is ruled out for the CO methanation on Rh catalyst at the reaction conditions used in this study. This is consistent with the lack of evidences for the direct dissociation of CO and CO disproportionation on Rh surfaces at temperatures below 600°C [6], but it disagrees with the direct C-O dissociation mechanism previously proposed on supported Rh catalysts [17,18]; therefore, a H-assisted C-O bond dissociation mechanism will be considered to explain the kinetic data shown in Fig.1, as discussed in section 3.3.

3.2. Infrared evidences for surface coverage at reaction conditions.

In order to study the predominant species adsorbed on the catalyst surface, self-supported catalysts wafers were studied by *in-situ* FTIR measurements at different CO and H_2 pressures. Fig.2 shows the main features observed in these experiments. A doublet appearing at

wavenumbers between 2100 and 2200 cm^{-1} is attributed to gas phase CO. The peaks appearing at lower wavenumbers are characteristic of adsorbed CO, which can be present in linear form (intense peak at ~ 2045 cm^{-1}) and bridged form (very broad peak located at ~ 1800 cm^{-1}). Other surface species such as carbonates, formates and CH_x were not present in significant quantities during the experiments and thus they are not shown here. Additionally, previous reports have shown that adsorbed CO is the main precursor of methane over Rh catalysts [6,10,13].

Linearly bonded CO preferentially dominates the Rh surface at the reaction conditions used in this study (Fig.2), in agreement with Rasband and Hecker report [21]. These authors also demonstrated that the ratio of linear to bridge CO surface concentration increased from 2 to 5 as Rh dispersion increase from 22 to 100%, while a very small effect of temperature on this ratio was observed between 50 and 200ºC [21]; the latter is consistent with the lack of changes in the area under CO peaks associated to linearly and bridged bonded species observed at temperatures below 200ºC in our IR measurements (see spectra at 130-200ºC in Fig.6, section 3.4), therefore, it was assumed that full CO* coverage of Rh surface was achieved at 200ºC for all the reactant partial pressures of CO used in this study. Consequently, the fractional coverage of linearly and bridged bonded CO* species on Rh was calculated from the averaged area under their peaks by using the integrated adsorption coefficients reported by Rasband and Hecker [21]; thus, the integrated adsorption intensity of linear CO peak from Figure 2 (peak at ~ 2045 cm^{-1}) was used to estimate the fractional coverage of Rh surface with linearly bonded CO. It is noteworthy that no noticeable deactivation during the *in-situ* FTIR experiments was observed at the reaction conditions reported in this work; it was confirmed by comparing the CO peak at the end and the beginning of the experiment at the same reaction condition after a series of measurements.

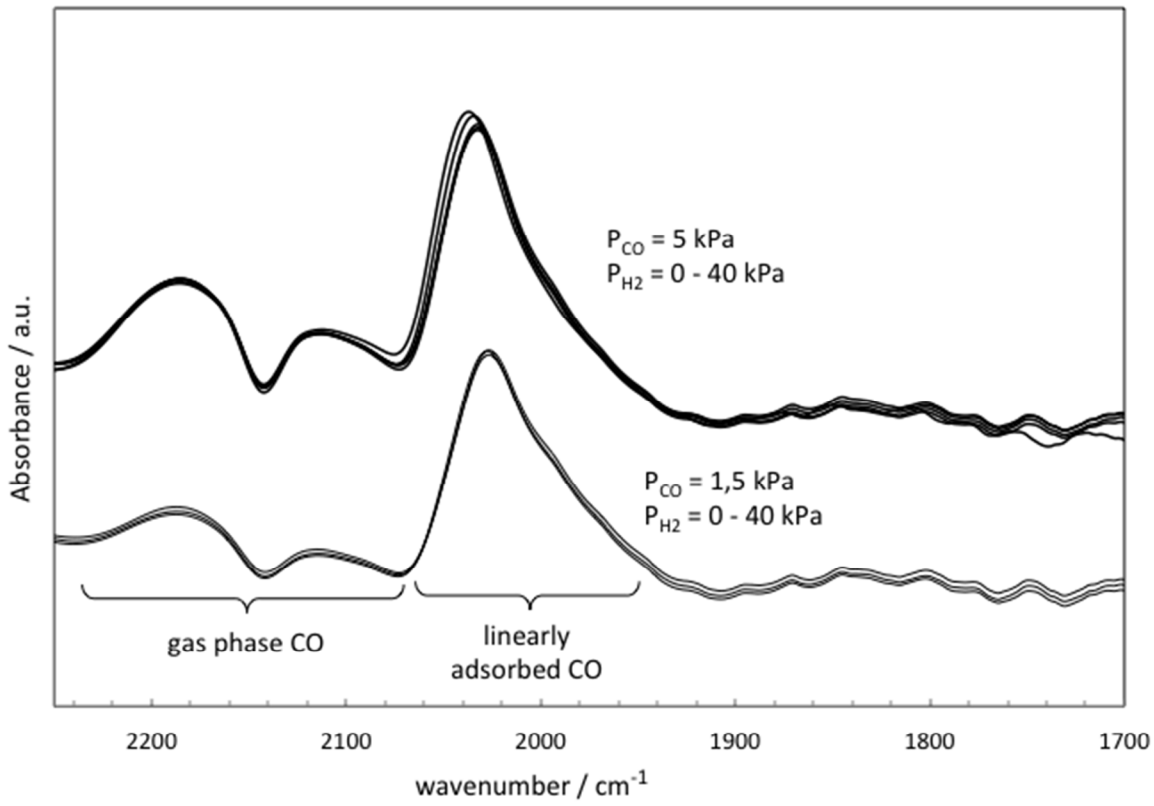

Figure 2. Infrared spectra recorded during CO hydrogenation on Rh/Al_2O_3 at 246°C. P_{CO} = 1.5 and 5 kPa, P_{H2} (0 – 40 kPa), P_{H2O} (0 – 1.6 kPa), space velocity 83.3 $cm^3 \cdot s^{-1} \cdot g_{cat}^{-1}$.

As shown in Figure 2, the peak areas for linearly bonded CO resulted independent of H_2 pressure. The estimated CO* coverage at different reactant composition is shown in Fig.3A, which demonstrate that CO* coverage is independent of H_2 pressure at the reaction conditions used in this study. These results indicate that the surface is dominated by adsorbed CO* species and that H* is not a MASI. Fisher and Bell [6] also observed that increasing the hydrogen partial pressure has no effect on the *in-situ* infrared spectra for CO hydrogenation at 548 K; however, they included the H* in the site balance of the rate expression for methane turnover rate formation. On the other hand, a decrease in CO coverage was observed when CO pressure was lowered from 5 kPa to 1.5 kPa at 246 ºC (Fig.3), which indicates that vacancies must also be considered in the site balance at these reaction conditions and that the full coverage of Rh surface with CO is a particular case for the site balance at lower temperatures. This is consistent with the model presented by Van Herwijnen et al. [7].

Furthermore, to evaluate whether the water formed during CO hydrogenation affects the surface coverage, infrared measurements were carried out in absence and presence of H_2O at a given CO and H_2 concentration in the feed (Fig.3B). It is observed that the presence of H_2O does not affect the coverage of CO*. Consequently, these results lead to conclude that neither H_2 nor H_2O affect the CO* coverage on Rh at the conditions studied.

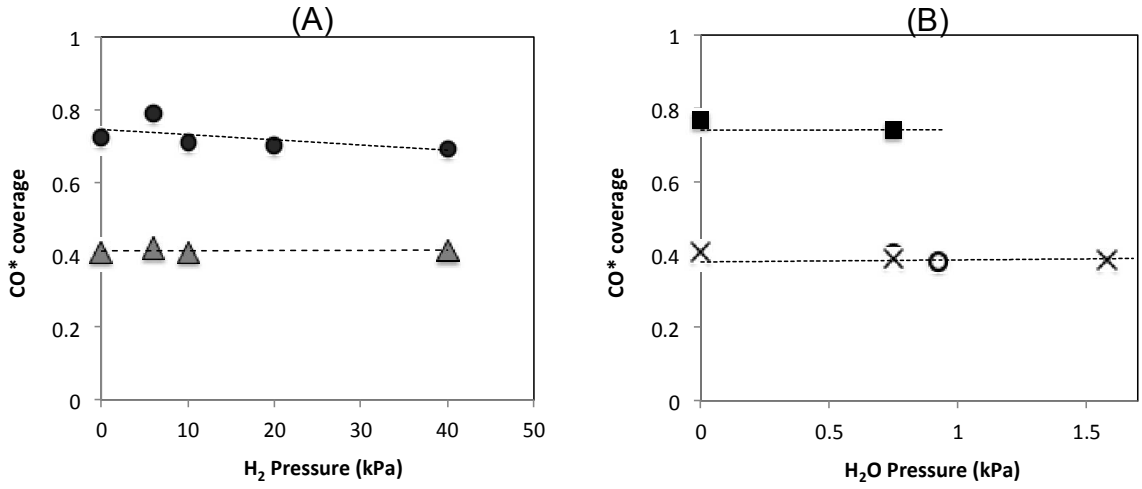

Figure 3. Surface coverage of carbon monoxide on Rh/Al_2O_3 at 246°C. (A) Effect of H_2 and CO pressures on CO* coverage: P_{H2} (0 – 40 kPa), (▲) 1.5 kPa CO and (●) 5 kPa CO; (B) Effect of H_2O pressure on CO* coverage: P_{H2O} (0 – 1.6 kPa), [(■) 5 kPa CO, 10 kPa H_2], [(○) 1.5 kPa CO, 10 kPa H_2], [(×) 1.5 kPa CO, 40 kPa H_2].

Thus, infrared experiments (Figures 2 and 3) demonstrate that Rh surface is dominated by vacancies and adsorbed CO* species ([*] + [CO*]) during CO hydrogenation on Rh catalysts at the reaction conditions used in this work.

3.3. Proposed sequence of elementary steps and Kinetics.

Since the kinetic data (Fig.1) are inconsistent with a direct C-O bond dissociation mechanism as discussed above, various H-assisted C-O bond dissociation mechanisms were considered to explain the H_2 and CO pressure effect on CH_4 formation rate. Scheme 2 and 3 represent the sequence of elementary steps in which the first or the second H* addition assists the C-O bond cleavage, respectively.

Kinetics represented by Eq.7 and Eq.8 are consistent with Scheme 2 and 3, respectively, where the vacancies and CO* coverage ($1 + \theta_{CO}$) conform the site balance, as evidenced by the *in-situ* infrared experiments shown in section 3.2. The molecular CO adsorption and the dissociative H_2 adsorption are considered quasi-equilibrated steps in these two mechanisms, which is consistent with previous reports for H_2 and CO adsorption on supported Rh catalysts at a similar range of reaction conditions [6,7,12,23]. K_{H2} and K_{CO} represent the equilibrium constants for these two steps, respectively.

Reaction Scheme 2.

2.1) $CO + * \rightleftharpoons CO*$
2.2) $H_2 + 2* \rightleftharpoons 2H*$
2.3) $CO* + H* \rightarrow C* + OH*$
2.4) $C* + H* \rightarrow CH* + *$
2.5) $CH* + H* \rightarrow CH_2* + *$
2.6) $CH_2* + H* \rightarrow CH_3* + *$
2.7) $CH_3* + H* \rightarrow CH_4* + *$
2.8) $CH_4* \rightarrow CH_4 + *$
2.9) $OH* + H* \rightarrow H_2O + 2*$
2.10) $OH* + CO* \rightarrow CO_2 + H* + *$

Scheme 2. H-assisted C-O bond dissociation mechanisms for CO hydrogenation on Rh/Al_2O_3; C-O bond dissociates after first H* addition.

$$r_{CH4} = \frac{k_{2.3}K_{CO}K_{H2}^{0.5}P_{CO}P_{H2}^{0.5}}{(1+K_{CO}P_{CO})^2} = \frac{\propto_2 \cdot P_{CO}P_{H2}^{0.5}}{(1+K_{CO}P_{CO})^2} \quad (7)$$

Reaction Scheme 3.

3.1) $CO + * \rightleftharpoons CO*$
3.2) $H_2 + 2* \rightleftharpoons 2H*$
3.3) $CO* + H* \rightleftharpoons HCO* + *$
3.4) $HCO* + H* \rightarrow CH* + OH*$
3.5) $CH* + H* \rightarrow CH_2* + *$
3.6) $CH_2* + H* \rightarrow CH_3* + *$
3.7) $CH_3* + H* \rightarrow CH_4* + *$
3.8) $CH_4* \rightarrow CH_4 + *$
3.9) $OH* + H* \rightarrow H_2O + 2*$
3.10) $OH* + CO* \rightarrow CO_2 + H* + *$

Scheme 3. H-assisted C-O bond dissociation mechanisms for CO hydrogenation on Rh/Al_2O_3; HCO* formation is quasi-equilibrated and CO bond cleavage occurs after the second H* addition.

$$r_{CH4} = \frac{k_{3.4}K_{HCO}K_{CO}K_{H2}P_{CO}P_{H2}}{(1+K_{CO}P_{CO})^2} = \frac{\propto_3 \cdot P_{CO}P_{H2}}{(1+K_{CO}P_{CO})^2} \quad (8)$$

According to Scheme 2, the first H* addition would assist the C-O bond cleavage. Following a Langmuir-Hinshelwood treatment of the surface reactions, this leads to the equation for the rate of methane formation shown in Eq. 7, which presents a 0.5 order with respect to P_{H2}. On the other hand, Eq.8 represents a mechanism in which the second H* addition provokes the C-O bond breaking in an irreversible step (Scheme 3), with all previous elementary steps quasi-equilibrated, including the surface reaction of HCO* formation (step 3.3); K_{HCO} represents the equilibrium constant for this step. It is noteworthy that both kinetic equations (Eq.7 and Eq.8) contain only two adjustable parameters (α and K_{CO}) and properly predict the positive effect of P_{H2} on reaction rate as well as the decrease in CH_4 formation rate with CO pressure (Fig.1); only the rate order with respect to H_2 pressure and the identity (physicochemical meaning) of parameters α_2 and α_3 are different between the two kinetic models.

The kinetic parameters (α and K_{CO}) at 200, 250 and 300ºC were fitted using the rate data and Equations 7 and 8 (see the values obtained in Table 1 at the end of this section). Solver tool of Excel was used to minimize the sum of relative errors (SRE) at each temperature through a non-linear parameter estimation protocol. Values for the total SRE are also shown in Table 1. The effect of temperature on kinetic parameters was evaluated in order to confirm their physicochemical meaning, therefore, the consistency of the proposed mechanisms (Scheme 2 and 3) and the corresponding kinetic model (Eq.7 and 8). The values of the parameters regressed from kinetic data are summarized in Table 1.

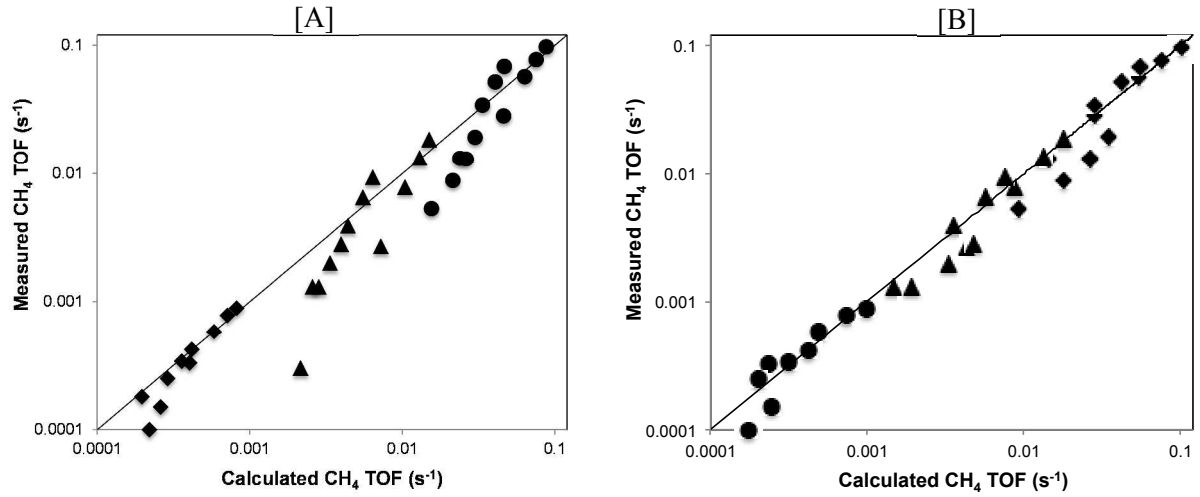

Figure 4. Parity plot for calculated ([A] Eq.7; [B] Eq.8) and measured CH_4 formation turnover rates (TOF) at 200ºC (●), 250ºC (▲) and 300ºC (♦) (1.0-7.1 kPa CO, 0-22.5 kPa H_2).

The parity plot shown in Fig.4A indicates that Eq.7 does not properly represent the kinetic data. Moreover, the effect of temperature on K_{CO} value, calculated from regression of Eq.7 with kinetic data (Table 1), is inconsistent with the physicochemical meaning expected for this parameter; since K_{CO} represents the equilibrium constant for CO adsorption on Rh surface, a decrease in the K_{CO} value with temperature is expected. Consequently, the mechanism in which C-O bond dissociates after first H* addition (Scheme 2 and Eq.7) can be disregarded based on physicochemical considerations.

On the other hand, the second H-addition mechanism modeled by Eq.8 seems to be consistent with the kinetic data (Fig.4B); moreover, the values obtained for parameters α_3 and K_{CO} are in agreement with the expected physicochemical meaning for them (Table 1).

The Arrhenius-type effect of temperature on α_3 leads to an apparent activation energy of 82.3 $kJ \cdot mol^{-1}$. According to Scheme 3 and Eq.8, α_3 contains the activation energy for the step 3.4, the energy associated to the equilibrated formation of HCO* (step 3.3), the enthalpy for the dissociative adsorption of H_2 (step 3.2) and the enthalpy of CO molecular adsorption (step 3.1), i.e., $E_{ap} = E_{3.4} + \Delta H_{HCO} + \Delta H_{H2} + \Delta H_{CO}$.

Also, the apparent activation energy was obtained from the Arrhenius plot of reaction rates measured at constant feed concentration (3 kPa CO, 10 kPa H_2) and 3 different temperatures; it leads to a value of $(E_{ap})_{rCH4}$ = 111 kJ/mol (Fig.5), which is fairly close to apparent activation

energies of 94.6 kJ/mol and 100.5 kJ/mol reported for 1%Rh/SiO_2 and 1%Rh/Al_2O_3, respectively [17], the 97.1 kJ/mol observed for the methanation on 3.4%Rh/SiO_2 [6] and the 100.5 kJ/mol reported for the CO hydrogenation on 1%Rh/Al_2O_3 [12]. The lower E_{ap} obtained from Arrhenius plot of α_3 as compared with $(E_{ap})_{rCH4}$ is attributed to the contribution of the enthalpy of CO adsorption in the denominator of Eq.8; the CO adsorption is an exothermic phenomenon ($\Delta H_{CO} < 0$) and the denominator is squared (Eq.8), therefore, $(E_{ap})_{rCH4} \sim E_{ap} - \Delta H_{CO}$, leading to a stronger effect of temperature on r_{CH4} than on parameter α_3.

The values for the enthalpy and entropy changes of CO adsorption on Rh surface were calculated from the slope and intercept of van't Hoff plot that represents the effect of temperature on the equilibrium constant K_{CO} (Eq.9), leading to $-\Delta H_{CO}$ = 14.1 kJ/mol and $-\Delta S_{CO}$ = 17.9 J/mol, respectively (Fig. 7). On the other hand, the heat of dissociative H_2 adsorption cannot be calculated from the kinetic data provided in this work because H* is not a MASI, therefore, no specific values for K_{H2} can be regressed from Eq.8. Also, the energetics of the surface equilibrated reaction for HCO* formation on Rh catalyst neither could be determined from the kinetic data presented in this work; only theoretical calculations would be able to estimate the energy involved in this surface reaction.

$$K_{CO} = e^{\frac{-\Delta G}{R \cdot T}} = e^{\frac{\Delta Sco}{R}} \cdot e^{\frac{-\Delta Hco}{R \cdot T}} \quad (9)$$

The negative value obtained for the ΔH_{CO} is consistent with the first criteria proposed by Boudart [34] to evaluate the validity of kinetic parameters, since it reflects the exothermic nature of the adsorption reaction. This value is lower than most of the previously reported values for the heat of CO adsorption on Rh catalysts (75-195 kJ/mol [24], 59-134 kJ/mol [25], 10-170kJ/mol [26]) and is attributed to the effect of coverage on ΔH_{CO}, which will be discussed in the section 3.4, where the enthalpy of CO adsorption calculated from *in-situ* FTIR measurements is compared with this ΔH_{CO} derived from kinetic data. Also, the value obtained for ΔS_{CO} is consistent with the second criteria ($0 < -\Delta S_{CO} < S^o_g$) [34] as the decrease in entropy after CO adsorption ($-\Delta S_{CO}$ = 17.9 $J \cdot mol^{-1} \cdot K^{-1}$) is lower than the entropy in gas phase (S^o_g = 197,6 $J \cdot mol^{-1} \cdot K^{-1}$). Consequently, the consistency and physicochemical meaning of the rate parameters calculated from kinetic data

ratify the validity of application of the Langmuir-Hinshelwood model to represent the reported kinetic data.

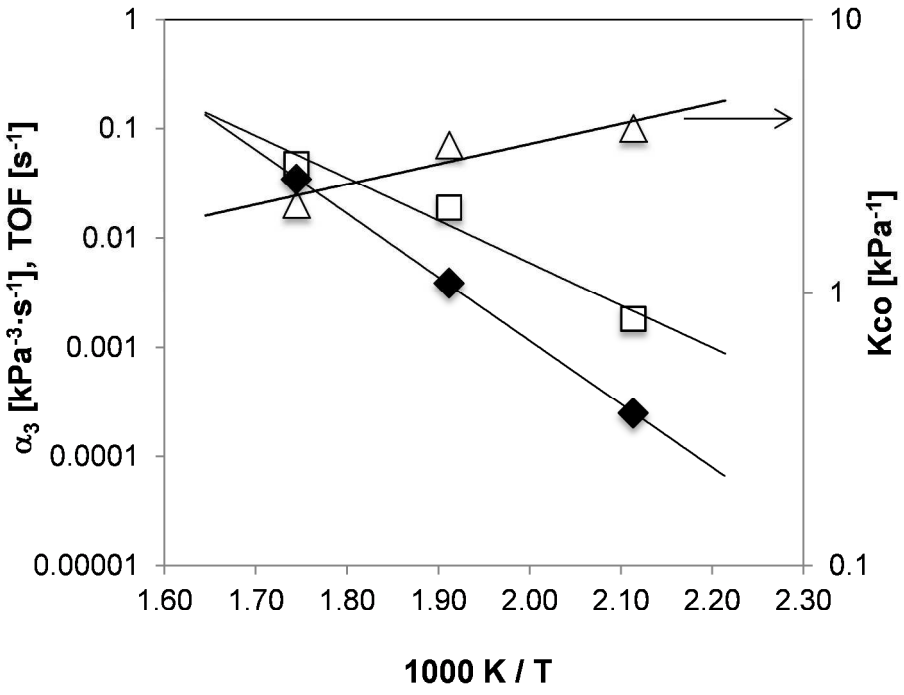

Figure 5. Effect of temperature on parameters (□) α_3, (Δ) K_{CO}. The physicochemical meaning of these parameters is provided though the Eq.8 and 9, respectively. (♦) Arrhenius plot of r_{CH4} (TOF, s^{-1}) measured at 3 kPa CO and 10 kPa H_2.

Table 1. Kinetic parameters for proposed reaction mechanisms and kinetics.

	Scheme 2 - Eq.7 CO* + H* → C* + OH*		Scheme 3 - Eq.8 HCO* + H* → CH* + OH*	
T (ºC)	α_2	K_{CO}	α_3	K_{CO}
200	0.0020	2.267	0.0018	3.981
250	0.0687	3.460	0.0198	3.594
300	0.1811	2.051	0.0922	3.298
E_{ap} (kJ·mol^{-1})	102.7	-	82.3	-
ΔH_{CO} (kJ·mol^{-1})	-	(‡)	-	-14.1
ΔS_{CO} (J·mol^{-1}·K^{-1})	-		-	-17.9

SRE^{++}	1004.0	785.9

(‡) The observed effect of temperature on K_{CO} is inconsistent with the physicochemical meaning of this parameter, since K_{CO} must decrease with temperature.

($^{++}$) The Sum of Relative Error at three temperatures: $SRE = \sum(\frac{|r_{exp}-r_{mod}|}{r_{mod}} \cdot 100)$.

3.4. Enthalpy of CO adsorption and temperature dependence of CO coverage calculated from infrared measurements on Rh surface.

The heat of CO adsorption can be estimated from *in-situ* infrared measurement and compared with the value calculated from van't Hoff plot of K_{CO} regressed from kinetic data (Fig.5/Table 1). A comparison of the values for this parameter obtained from two independent measurements on the same catalysts at similar reaction conditions can provide valuable information in order to assess the physicochemical meaning of this parameter and to validate the H-assisted mechanism and Kinetics proposed above for the CO methanation reaction.

In order to estimate the heat of CO adsorption on Rh catalyst as a function of CO* coverage, the change in the area of linearly bonded and bridge CO peaks was quantified by *in-situ* FTIR measurements as a function of temperature (130-300ºC) at constant reactant gas composition (5 kPa CO, 10 kPa H_2, balance He, 100 ml·min^{-1}). The figure inserted into Fig.6A shows that CO* coverage is practically constant up to 200ºC and decreases as the temperature increases from 200ºC to 300ºC. As explained above, the fractional coverage of linearly and bridged bonded CO* species on Rh as a function of temperature was calculated from the averaged area under their peaks by using the integrated adsorption coefficients reported by Rasband and Hecker [21]; since the ratio of linear to bridge CO surface coverage $\frac{[CO*]_L}{[CO*]_B}$ resulted higher than 9 for the used conditions, only the coverage of linearly bonded CO* species was considered to calculate the equilibrium constant (K_{CO}) for CO adsorption on Rh/Al_2O_3 catalyst as a function of temperature (Fig.6A). It is also observed that the peak associated to linearly adsorbed CO* species moves to higher wavenumbers as the temperature decreases (Figure inserted into Fig.6A); it is attributed to the increase of CO* coverage, which weakens the Rh-CO interaction and, consequently, leads to an increase in the frequency of C-O bond vibration.

The values for equilibrium constant (K_{CO}) at different temperatures were calculated from *in-situ* FTIR measurements by using the Langmuir model (Eq.10). The differential form of van't Hoff

equation (Eq.11) was used to calculate the enthalpy of CO adsorption as a function of CO* coverage (θ_{CO}).

$$K_{CO} = \left(\frac{P_0}{P}\right)\frac{\theta_{CO}}{(1-\theta_{CO})} \quad (10)$$

$$\frac{dlnK_{CO}}{d\frac{1}{T}} = -\frac{\Delta H_{CO}}{R} \quad (11)$$

The values for the equilibrium constant of CO adsorption calculated from *in-situ* FTIR measurements (Eq.10) and from kinetic data (Eq.8) are compared in Fig.6B. A great similarity is observed between both values at the evaluated temperature range.

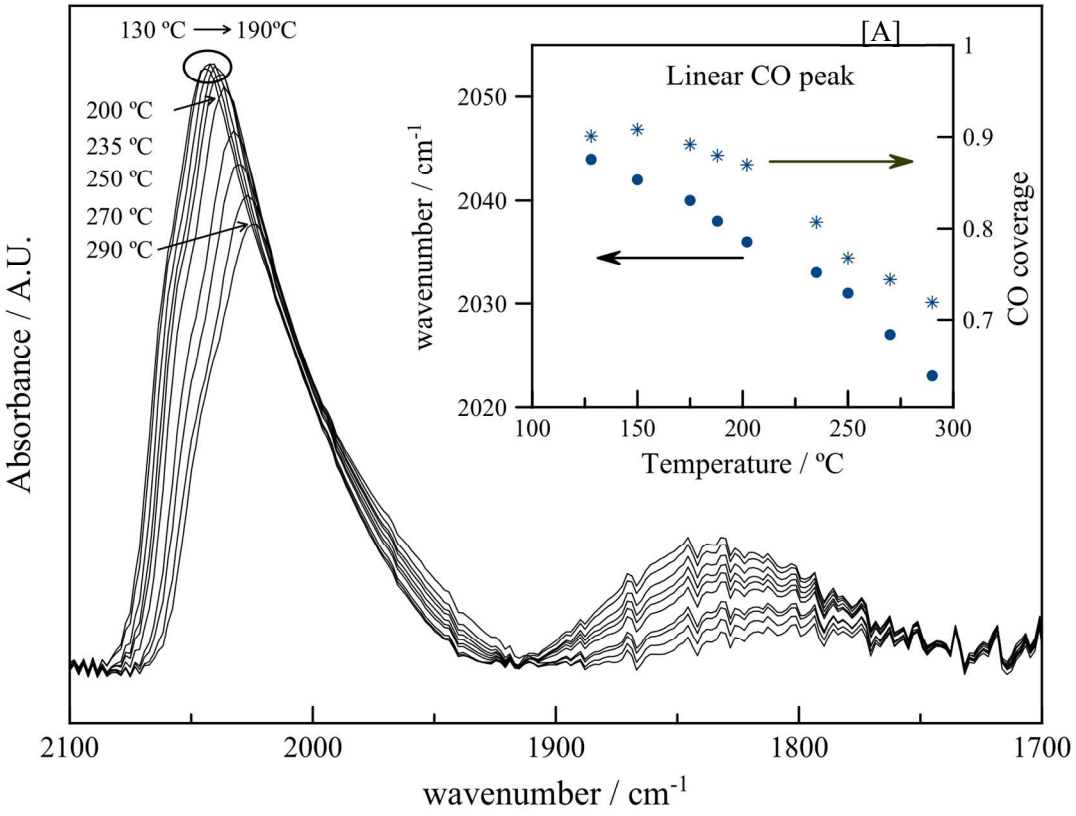

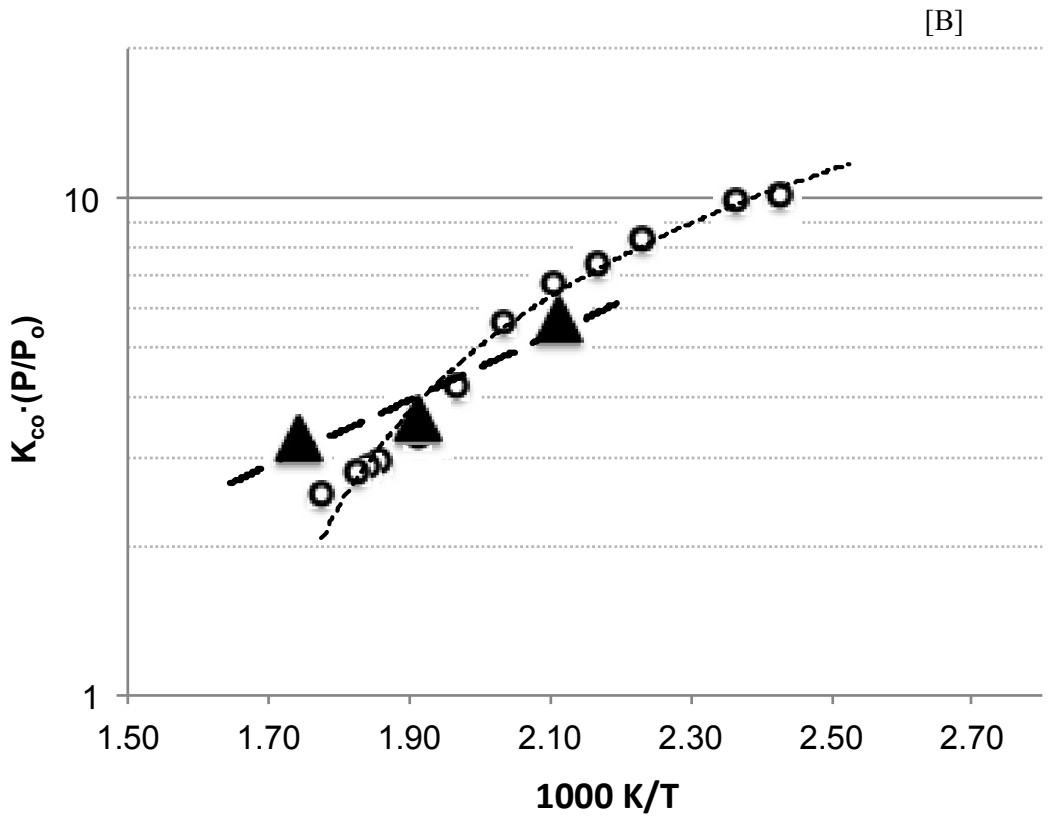

Figure 6. Infrared measurements for CO adsorption on Rh catalysts as a function of temperature (5 kPa CO, 10 kPa H_2, balance He, 100 ml·min^{-1}): (A) IR peaks for linearly bonded CO (θ_L, peak at ~ 2045 cm^{-1}) and bridge-bonded CO (θ_B, peak at ~ 1830 cm^{-1}); (B) Equilibrium constant for CO adsorption as a function of temperature calculated from: (o) FTIR measurements, (▲) kinetic data.

The enthalpy of CO adsorption on Rh catalyst was calculated as a function of CO* coverage (Fig.7). The decrease of CO* coverage with temperature is consistent with the exothermic nature of CO adsorption phenomenon. Fisher and Bell [6] observed a weaker effect of temperature on linearly bonded CO coverage, which decreased from 0,82 to 0.71 as the temperature increased from 50 to 300ºC during infrared measurements on Rh/SiO_2 at 250 Torr CO and no H_2 in the feed.

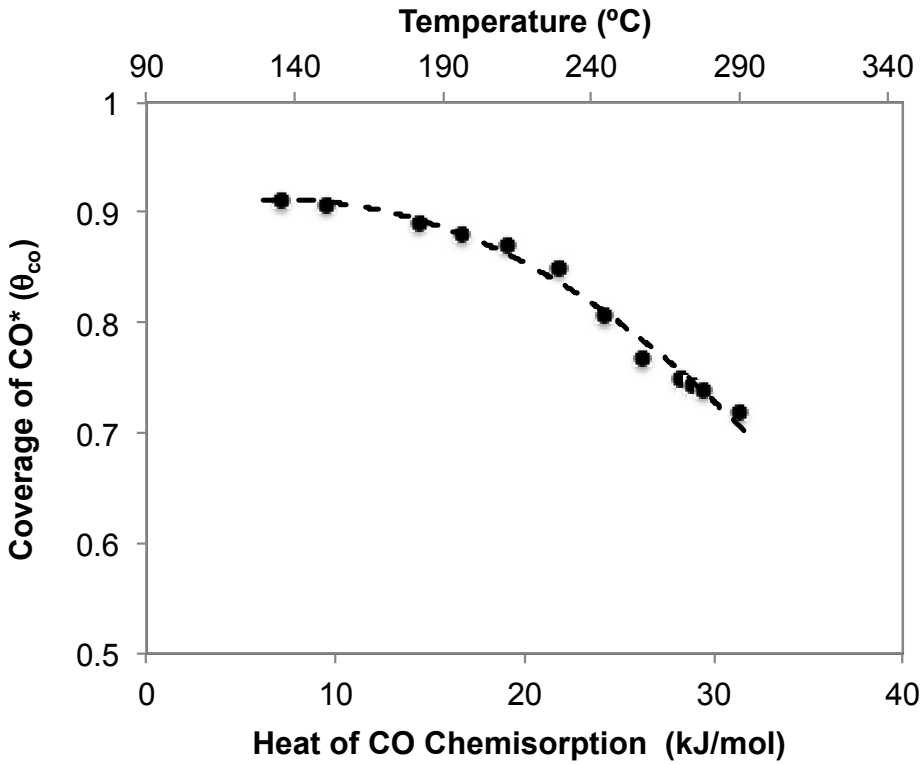

Figure 7. Heat of CO adsorption on Rh/Al_2O_3 catalyst as a function of temperature (200–300ºC) and linearly bonded CO* coverage calculated from FTIR measurements (5 kPa CO, 10 kPa H_2, balance He, 100 ml·min^{-1}).

A constant value for the heat of CO adsorption (ΔH_{CO} = -14.1 kJ/mol) is obtained from van't Hoff plot of K_{CO} regressed from kinetic data, since this parameter is assumed independent of CO* coverage. On the other hand, the enthalpy of CO adsorption calculated from infrared experiments ranges between -5 and -31 kJ/mol and is affected by the CO* coverage of Rh surface (Fig.7), which is congruent with previous reports [24,26]. In fact, Maroto-Valiente et al. also report a decrease in the enthalpy of CO adsorption on Al_2O_3-supported 1%Rh catalyst from 120 kJ/mol to 30 kJ/mol as CO* coverage increases from 0.2 to full coverage [26]. It is noteworthy that the value for ΔH_{CO} calculated from kinetic data is within the range of ΔH_{CO} values calculated from FTIR measurements.

Also, the *in-situ* FTIR measurements show that high CO* coverage on Rh surface (Fig.7) corresponds to lower values for the heat of CO adsorption (ΔH_{CO} ~ 20 kJ/mol at 200-220ºC); this value is slightly lower than the 59 kJ/mol and 75 kJ/mol reported by Seebauer et al. [25] and

Dulaurent et al. [24], respectively, for a Rh surface fully covered with CO, but it is fairly close to the range 10-40 kJ/mol observed by Maroto-Valiente et al. [26] for the CO adsorption on 1%Rh/Al_2O_3 at high coverage. At higher temperatures (250-300ºC) the CO* coverage significantly decreases as a consequence of the exothermic character of CO adsorption, leading to an increase in the calculated enthalpy of CO adsorption (Fig.7); the infrared data predict a value of ~100 kJ/mol for ΔH_{CO} at CO* coverage near to 0.1, lying near the range 125-195 kJ/mol reported by Dulaurent et al. [24] for bare Rh surface; also, this value is close to the 134 kJ/mol observed by Seebauer et al. [25] at lower CO* coverage and it is also fairly consistent with the range informed by Maroto-Valiente et al. [26] for CO adsorption on 1%Rh/Al_2O_3 at low coverage.

It is important to note that the heat of CO adsorption calculated from *in-situ* FTIR experiments by quantifying the change in CO coverage with temperature, resulted independent of H_2 pressure (Fig.2 and 3); conversely, kinetic data show a strong effect of P_{H2} on reaction rates (Fig.1). This suggests that the ΔH_{CO} calculated from FTIR measurements represents all Rh surface sites; regardless which part of this Rh surface is more active for CH_4 formation. On the other hand, the value of ΔH_{CO} calculated from kinetic data represents the surface that is actually performing the catalytic turnover. Even though the FTIR experiments show the CO adsorption over the whole Rh surface regardless its activity, the proper combination of IR analysis and kinetic measurements suggest that only a fraction of exposed surface is effectively catalyzing the CO hydrogenation.

The lower values for ΔH_{CO} are usually related to higher metal coordination in low-index faces of metal clusters [15,27,28]; therefore, the relatively lower ΔH_{CO} value obtained from kinetic model as compared with FTIR evidences, suggests that the kinetic data is dominated by the higher activity of more coordinated Rh surface atoms prevalent in open surfaces. A plausible conclusion would be that CH_4 formation rate from CO hydrogenation is favored over large clusters, which present a larger fraction of low-index facets. This expected structure sensitivity is consistent with previous reports for the methanation reaction on supported Rh catalyst [15,29,30]. Mori at al. [15] combined pulse surface reaction rate analysis (PSRA) and FTIR measurements to show that C-O bond dissociation and CH_x hydrogenation rates increase with decreasing of Rh dispersion. Moreover, authors observed that the wavenumber of liner CO decreases with increasing Rh dispersion in Rh/Al_2O_3 catalysts [15], which indicates that CO adsorbs stronger on small Rh particles; therefore, a lower values for ΔH_{CO} is expected for CO adsorption on larger Rh particles. Also, Karelovic et al. [10] observed higher CH_4 formation rates on larger Rh particles for the CO_2

hydrogenation; since CO and CO_2 hydrogenations are proposed to share similar mechanisms [6], the structure sensitivity observed for CO_2 methanation could also be the case for CO hydrogenation over supported Rh. Carballo et al. [27] reported higher CO conversion rates on larger Ru clusters and a similar cluster size effect for the same reaction over supported cobalt catalyst have been informed by Bezemer et al. [31]. Kinetic and *in-situ* FTIR measurements for the methanation reaction on Rh catalysts with different cluster size must be performed in order to confirm the structure sensitivity suggested above.

4. CONCLUSIONS

The hydrogenation of CO to produce methane on Rh/Al_2O_3 has been studied. Kinetic and *in-situ* FTIR evidences support a mechanism in which the C-O bond cleavage occurs in an irreversible step assisted by a second H-addition, with all previous elementary steps quasi-equilibrated, including the surface reaction of HCO* formation. I*n-situ* Infrared measurements demonstrate that CO* species and vacancies dominate the Rh surface and ruled out the H* and H_2O as a MASI, during CO hydrogenation at the reaction conditions studied. A Langmuir-Hinshelwood model is proposed for CH_4 formation rate, which is consistent with kinetic data. The physicochemical meaning of the kinetic parameters is confirmed. It is demonstrated that the CO* coverage of Rh surface affects the heat of CO adsorption.

ACKNOWLEDGEMENTS

The authors gratefully acknowledge the support of FONDECYT Grant 1140410 (RJ), 1120363 (FG), PAI-CONICYT 79130023 Grant (AK) and Technological Development Unit (UDT) of the Universidad de Concepción, Basal Project PFB-27. RJ also thanks Professor Enrique Iglesia (UCB) for valuable discussions.

REFERENCES

[1] Andersson, M. P.; Bligaard, T.; A. Kustov, A.; Larsen, K. E.; Greeley, J.; Johannessen, T.; Christensen, C. H.; Norskov, J. K.; *J. Catal.* **2006,** 239, 501-506.
[2] Ponec, V.; *Catal. Rev.* **1978**, 18,151-171.
[3] Vannice, M. A.; *J. Catal.* **1977**, 50, 228-236.
[4] Nørskov, J. K.; Bligaard, T.; Logadottir, A.; Bahn, S.; Hansen, L. B.; Bollinger, M.; Bengaard, H.; Hammer, B.; Sljivancanin, Z.; Mavrikakis, M.; Xu, Y.; Dahl, S.; Jacobsen, C. *J. Catal.* **2002**, 209, 275-278.

[5] Kustov, A. L.; Frey, A. M.; Larsen, K. E.; Johannessen, T.; Nørskov, J. K.; Christensen, C. H. *Appl. Catal., A* **2007**, 320, 98-104.
[6] Fisher, I. A.; Bell, A. T. *J. Catal.* **1996**, 162, 54-65.
[7] Van Herwijnen, T.; Van Doesburg, H.; De Jong, W. A. *J. Catal.* **1973**, 28, 391-402.
[8] Mori, T.; Masuda, H.; Imai, H.; Miyamoto, A.; Baba, S.; Murakami, Y. *J. Phys. Chem.* **1982**, 86, 2753-2760.
[9] Sehested, J.; Dahl, S.; Jacobsen, J.; Rostrup-Nielsen, J. R. *J. Phys. Chem. B* **2004**, 109, 2432-2438.
[10] Karelovic, A.; Ruiz, P. *J. Catal.* **2013**, 301, 141-153.
[11] Henderson, M. A.; Worley, S. D. *J. Phys. Chem.* **1985**, 89, 1417-1423.
[12] Vannice, M. A. *J. Catal.* **1975**, 37, 462-473.
[13] Karelovic, A.; Ruiz, P. *Appl. Catal., B* **2012**, 113–114, 237-249.
[14] Ishikawa, A.; Iglesia, E. *J. Catal.* **2007**, 252, 49-56.
[15] Mori, Y.; Mori, T.; Miyamoto, A.; Takahashi, N.; Hattori, T.; Murakamit, Y. *J. Phys. Chem.* **1989**, 93, 2039-2043.
[16] Shetty, S.; van Santen, R. A. *Catal. Today* **2011**, 171, 168-173.
[17] Solymosi, F.; Tombácz, I.; Kocsis, M. *J. Catal.* **1982**, 75, 78-93.
[18] Iizuka, T.; Tanaka, Y.; Tanabe, K. *J. Catal.* **1982**, 76, 1-8.
[19] Panagiotopoulou, P.; Kondarides, D. I.; Verykios, X. E. *Appl. Catal., A* **2008**, 344, 45-54.
[20] Claeys, M.; van Steen, E. *Catal. Today* **2002**, 71, 419-427.
[21] Rasband, P. B.; Hecker, W. C. *J. Catal.* **1993**, 139, 551-560.
[22] Madon, R. J.; Boudart, M. *Ind. Eng. Chem. Fundam.* **1982**, 21, 438-447.
[23] Williams, K. J.; Boffa, A. B.; Salmeron, M.; Bell, A. T.; Somorjai, G. A. *Catal. Lett.* **1991**, 9, 415-426.
[24] Dulaurent, O.; Chandes, K.; Bouly, C.; Bianchi, D. *J. Catal.* **2000**, 192, 262-272.
[25] Seebauer, E. G.; Kong, A. C. F.; Schmidt, L. D. *Appl. Surf. Sci.*, **1988**, 31, 163-172.
[26] Maroto-Valiente, A.; Rodríguez-Ramos, I.; Guerrero-Ruiz, A. *Catal. Today* **2004**, 93–95 567-574.
[27] Carballo, J. M. G.; Yang, J.; Holmen, A.; García-Rodríguez, S.; Rojas, S.; Ojeda, M.; Fierro, J. L. G. *J. Catal.* **2011**, 284, 102-108.
[28] den Breejen, J. P.; Radstake, P. B.; Bezemer, G. L.; Bitter, J. H.; Frøseth, V.; Holmen, A.; de Jong, K. P. *J. Am. Chem. Soc.* **2009**, 131, 7197-7203.
[29] Boudart, M.; McDonald, M. A. J. *Phys. Chem.* **1984**, 88, 2185-2195.
[30] Underwood, R. P.; Bell, A. T. *Appl. Catal.* **1987**, 34, 289-310.
[31] Bezemer, G. L.; Bitter, J. H.; Kuipers, H. P. C. E.; Oosterbeek, H.; Holewijn, J. E.; Xu, X.; Kapteijn, F.; van Dillen, A. J.; de Jong, K. P. *J. Am. Chem. Soc.* **2006**, 128, 3956-3964.
[32] Orita, H.; Naito, S.; Tamaru, K.; *J. Catal.* **1988**, 111, 464-467.
[33] Wei, J; Iglesia, E.; *J. Catal.* **2004**, 225, 116-127.
[34] M. Boudart AICHE J. 18 (1972) 465-478

GRAPHICAL ABSTRACT

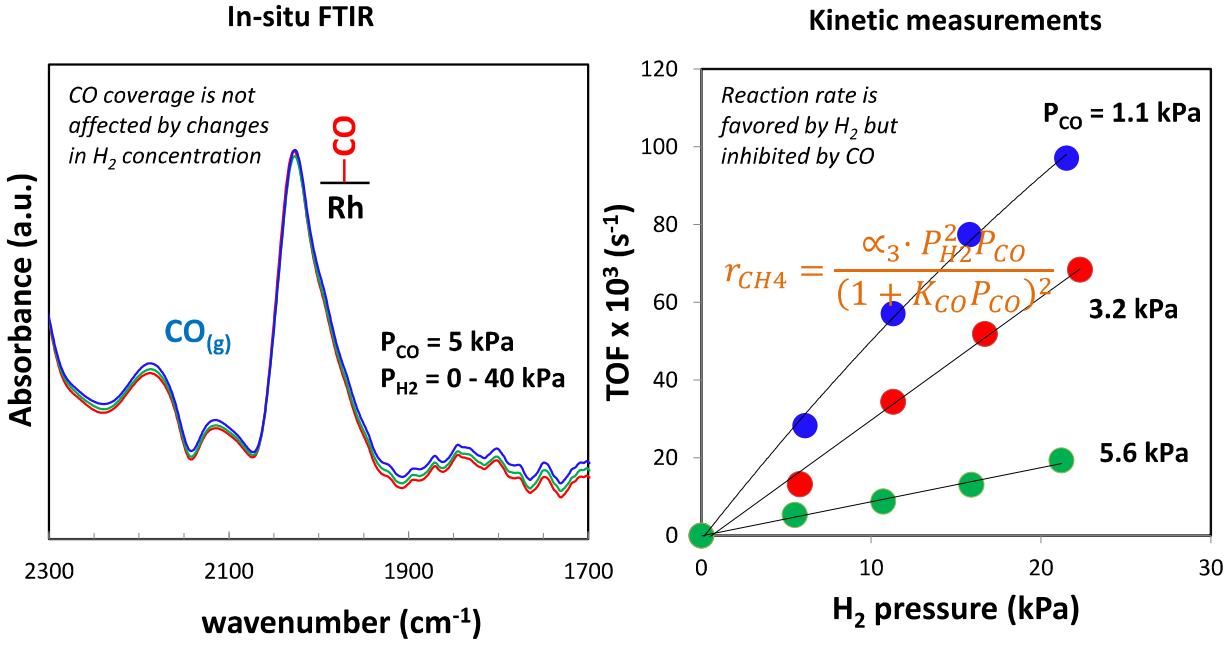

$$r_{CH4} = \frac{\propto_3 \cdot P_{H2}^2 P_{CO}}{(1 + K_{CO} P_{CO})^2}$$